8.5
Relative Orbits

Having explored the conditions for a general transfer between orbits, the more delicate problem is to meet a target point in the final orbit, a so-called orbital rendezvous. In this and the next section, we will focus on orbital rendezvous in Earth orbits though the described methods apply to any planetary orbit. For interplanetary orbital rendezvous, we refer the reader to Section 9.3.

In orbital rendezvous, there is generally a passive target object to rendezvous with an interceptor (a.k.a. *chaser*) as the active part that performs the rendezvous maneuvers. Rather than describe the required rendezvous maneuvers in an inertial reference frame such as a geocentric reference frame, it is very convenient to describe them relative to the target. It is convenient because if the interceptor moves in the vicinity of the target, we can linearize the equations of motion, which will enable us to solve them analytically. On the other hand, the target in a conical motion about the center of gravity constitutes a non-inertial reference system, a fact that will complicate our equation of motion somewhat. Nevertheless, the description of relative motion about a target object, which is done in the following, is a prerequisite for analyzing rendezvous maneuvers, which is the objective of Section 8.6.

8.5.1
General Equation of Motion

Suppose there is a target object in a planetary orbit and a S/C, the chaser, wants to navigate in its vicinity and with respect to it. Good examples are the approach maneuvers of a Soyuz vehicle to the ISS or the re-docking of the ascending Lunar Module to the Command/Service Module in low Lunar orbit during the Apollo moon missions. For this mission, we need to know the relative motion to the target and how to maneuver to reach the target. This is the subject of the next two sections.

Let us assume the target (for instance, we assume the ISS) is in an arbitrary terrestrial conic orbit with position vector $\boldsymbol{R}$ in the geocentric reference frame. For this orbit, Newton's equation of motion (7.1.19) must hold

$$\ddot{\boldsymbol{R}} = -\frac{\mu}{R^3}\boldsymbol{R} \tag{8.5.1}$$

Of course, Newton's equation of motion must equally hold for the chaser's orbit with position vector $\boldsymbol{\varrho}$ in the geocentric reference frame, i.e.,

$$\ddot{\boldsymbol{\varrho}} = -\frac{\mu\boldsymbol{\varrho}}{\varrho^3}$$

We start deriving the chaser's equation of motion relative to the ISS by defining the relative vector $\boldsymbol{r} = \boldsymbol{\varrho} - \boldsymbol{R}$ as shown in Figure 8.19. The specific reference frame is

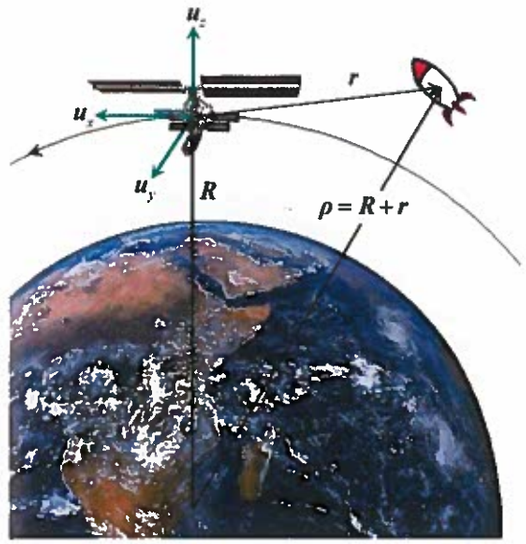

Figure 8.19 Definition of relative vectors and RSW reference system in the target object (ISS) that moves on a circular orbit. The z-axis points along the radial vector, while the x-axis points along the moving direction of the target object. The y-axis completes the right-handed reference system.

the ISS-centric reference system RSW as described in Section 13.1 (Figure 13.4) with unit vectors $\boldsymbol{u}_x, \boldsymbol{u}_y, \boldsymbol{u}_z = \boldsymbol{S}, \boldsymbol{W}, \boldsymbol{R}$: The z-axis points along the radial vector, while the x-axis points along the moving direction of the target. The y-axis completes the right-handed reference system. Our goal is to find the equation of motion of the relative vector

$$\boldsymbol{r} = \boldsymbol{\varrho} - \boldsymbol{R} = x\boldsymbol{u}_x + y\boldsymbol{u}_y + z\boldsymbol{u}_z =: (x, y, z)$$

as described in the non-inertial reference system $\boldsymbol{u}_x, \boldsymbol{u}_y, \boldsymbol{u}_z$. Since we seek for a differential equation for $\boldsymbol{r}$, we first have to express $\boldsymbol{\varrho}$ in terms of $\boldsymbol{R}$ and $\boldsymbol{r}$. Because $r \ll R$, we can expand the term $1/\varrho^3$ as follows:

$$\frac{1}{\varrho^3} = \frac{1}{[x^2 + y^2 + (z+R)^2]^{3/2}} \approx \frac{1}{(z+R)^3} \approx \frac{1}{R^3}\frac{1}{(1+z/R)^3} \approx \frac{1}{R^3}\left(1 - 3\frac{z}{R}\right)$$

and hence

$$\ddot{\boldsymbol{\varrho}} = \frac{-\mu\boldsymbol{\varrho}}{\varrho^3} \approx -\frac{\mu}{R^3}(\boldsymbol{R} + \boldsymbol{r})\left(1 - 3\frac{z}{R}\right) \approx -\frac{\mu}{R^3}(\boldsymbol{R} + \boldsymbol{r} - 3z\boldsymbol{e}_z)$$

Because from the definition of ϱ and from Eq. (8.5.1) also $\ddot{\varrho} = \ddot{R} + \ddot{r} = -\mu R/R^3 + \ddot{r}$ holds, we get

$$-\frac{\mu}{R^3}R + \ddot{r} \approx -\frac{\mu}{R^3}(R + r - 3ze_z)$$

and finally

$$\ddot{r} = -\frac{\mu}{R^3}(r - 3ze_z) \qquad @\ x, y, z \ll R \tag{8.5.2}$$

This equation of motion for r is close to, but not quite, what we want: Because the reference system rotates in the x–z plane and the unit vectors are time dependent, $u_x(t), u_y, u_z(t)$, the acceleration vector

$$\ddot{r}|_r = \frac{d^2}{dt^2}\left[x u_x(t) + y u_y + z u_z(t)\right]$$

comprises time derivates of the unit vectors, namely, $\dot{u}_x, \dot{u}_z$ and $\ddot{u}_x, \ddot{u}_z$, that we have to express in terms of our reference system u_x, u_y, u_z. The corresponding well-known transformation equations for an arbitrary vector a in a rotating frame with rotation vector ω are given by mathematical textbooks as

$$\dot{a}|_r = \dot{a}_i + \omega \times a$$
$$\ddot{a}|_r = \ddot{a}|_i + 2\omega \times \dot{a}|_i + \omega \times (\omega \times a) + \dot{\omega} \times a$$

with

$$\dot{a}|_i := \dot{a}_x u_x + \dot{a}_y u_y + \dot{a}_z u_z$$
$$\ddot{a}|_i := \ddot{a}_x u_x + \ddot{a}_y u_y + \ddot{a}_z u_z$$

For our purposes $a = r = (x, y, z)$ and $\omega = \omega(0, 1, 0)$, and therefore we obtain for the $\ddot{r}$ vector

$$\ddot{r}|_r = \ddot{r}|_i + \overbrace{2\omega \times \dot{r}|_i}^{\text{Coriolis force}} + \overbrace{\omega \times (\omega \times r)}^{\text{centrifugal force}} + \dot{\omega} \times a$$
$$= (\ddot{x} + 2\omega\dot{z} - \omega^2 x + \dot{\omega}z)u_x + \ddot{y}u_y + (\ddot{z} - 2\omega\dot{x} - \omega^2 z - \dot{\omega}x)u_z$$
$$= \begin{pmatrix} \ddot{x} + 2\omega\dot{z} - \omega^2 x + \dot{\omega}z \\ \ddot{y} \\ \ddot{z} - 2\omega\dot{x} - \omega^2 z - \dot{\omega}x \end{pmatrix}$$

If we insert this into Eq. (8.5.2), we finally obtain the equation of motion in column notation

$$\ddot{r} = \begin{pmatrix} \ddot{x} + 2\omega\dot{z} - \omega^2 x + \dot{\omega}z \\ \ddot{y} \\ \ddot{z} - 2\omega\dot{x} - \omega^2 z - \dot{\omega}x \end{pmatrix} = -\frac{\mu}{R^3}\begin{pmatrix} x \\ y \\ z - 3z \end{pmatrix}$$

Because this vectorial equation must hold for each orthogonal component separately, we finally find three differential equations

$$\begin{aligned} \ddot{x} + 2\omega\dot{z} - \left(\omega^2 - \frac{\mu}{R^3}\right)x + \dot{\omega}z &= 0 \\ \ddot{y} + \frac{\mu}{R^3}y &= 0 \\ \ddot{z} - 2\omega\dot{x} - \left(\omega^2 + 2\frac{\mu}{R^3}\right)z - \dot{\omega}x &= 0 \end{aligned} \qquad @\ x, y, z \ll R \quad \textbf{equations of motion} \tag{8.5.3}$$

This are the equations of motion of a chaser, not being subject to external forces, relative to a target with coordinates (x, y, z) in the target's topocentric RSW reference system, which quite generally is in a conic orbit about a center of gravity and, due to its conical trajectory, rotates with momentary orbital frequency $\omega(t)$.

Note that only the first and third equations are coupled. If initially $y(0) = 0$ and $\dot{y}(0) = 0$, i.e., if the chaser initially is in the orbital plane, then $\ddot{y} = 0$ and hence $y(t) = 0$, which means that it will always stay in that plane. Otherwise it will oscillate about this plane with frequency $\omega = \sqrt{\mu/R^3}$ if $R \approx const$ within the orbital period.

Elliptic Target Orbit

To get more practical and to find a solution to Eq. (8.5.3), we now assume an elliptic orbit with Keplerian elements a, e about a planet. For this, we get according to Eq. (7.2.5)

$$\omega = \dot{\theta} = \frac{\sqrt{\mu a(1 - e^2)}}{R^2}$$

and with Eqs. (7.3.8) and (7.4.13c)

$$\dot{\omega} = -2\frac{\mu e \sin\theta}{R^3} = -\frac{2\mu a e}{R^4}\sqrt{1 - e^2}\sin E$$

with

$$R(t) = a[1 - e\cos E(t)]$$

where the eccentric anomaly $E(t)$ is the solution of Kepler's equation (7.4.16)

$$n \cdot t = t\sqrt{\frac{\mu}{a^3}} = E(t) - e\sin E(t)$$

This transcendental equation can be solved by Newton's iteration method (Eq. (7.4.17))

$$E_{i+1} = E_i - \frac{E_i - e\sin E_i - n\cdot t}{1 - e\cos E_i}$$

Of course, similar equations can easily be derived for a hyperbolic trajectory (cf. Section 7.4.4).

Given these time-dependent quantities, the differential equations (8.5.3) for a rendezvous on an elliptic target orbit can be solved numerically, for instance, by a Runge–Kutta method.

Small Eccentricities

For small eccentricities, it is easy to show (exercise) that Eqs. (8.5.3) pass over into

$$\begin{aligned} \ddot{x} + 2n\dot{z} &= en[nx\cos nt + 2nz\sin nt - 4\dot{z}\cos nt] \\ \ddot{y} + n^2 y &= -3en^2 y\cos nt \qquad @\ e \ll 1 \\ \ddot{z} + 2n\dot{x} - 3n^2 z &= 2en[-nx\sin nt + 5nz\cos nt + 2\dot{x}\cos nt] \end{aligned} \tag{8.5.4}$$

with

$$n = \sqrt{\frac{\mu}{a^3}}$$

These equations can be solved directly with an appropriate solver for differential equations.

8.5.2 Hill's Equations

We now come to the most common situation where the target is in a circular orbit. Circular orbits are so common because for a given minimum altitude they have the lowest orbital energy, entailing the least delta-v to achieve. Therefore, nearly every target in a low Earth orbit (LEO) will attain a circular or near-circular orbit. For instance, the ISS has an eccentricity of typically $e = 0.0001-0.001$ that can be shown to be induced by the anisotropies of Earth's gravitational potential (see Section 12.3.2).

For a circular orbit, we have $\ddot{\boldsymbol{R}} = -\mu\boldsymbol{R}/R^3 = -n^2\boldsymbol{R}$ and $n = \sqrt{\mu/R^3} = 2\pi/T = const.$ If we insert this into the general equation of motion Eq. (8.5.3) or alternatively set $e = 0$ in Eq. (8.5.4), we obtain

$$\boxed{\begin{aligned} \ddot{x} + 2n\dot{z} &= 0 \\ \ddot{y} + n^2 y &= 0 \\ \ddot{z} - 2n\dot{x} - 3n^2 z &= 0 \end{aligned}} \quad @\ x, y, z \ll R \quad \textbf{Hill's equations} \tag{8.5.5}$$

These are the famous *Hill's equations* (a.k.a. *Clohessy–Wiltshire equations*) governing the motion of a S/C, not being subject to external forces, with coordinates (x, y, z) in the topocentric RSW reference system of a target object circling a planet with constant orbital frequency $\omega = n$.

Solution of Hill's equations

To describe the explicit motion $r(t) = (x(t), y(t), z(t))$ of the chaser, we have to solve Hill's equations. This can be done straightforwardly with only little effort. To do so efficiently, we define the initial conditions at $t = 0$ as

$$\begin{aligned} x(0) &= x_0,\ \dot{x}(0) = \dot{x}_0 \\ y(0) &= y_0,\ \dot{y}(0) = \dot{y}_0 \\ z(0) &= z_0,\ \dot{z}(0) = \dot{z}_0 \end{aligned}$$

and for the time being the quantities

$$\begin{aligned} x_{0n} &:= \dot{x}_0/n \\ y_{0n} &:= \dot{y}_0/n \\ z_{0n} &:= \dot{z}_0/n \end{aligned}$$

First, observe that the second Hill equation is decoupled from all others. It has the form of a harmonic oscillator. We therefore find its solution as

$$y = y_0\cos nt + y_{0n}\sin nt$$

We now integrate the first Hill equation directly. By taking the initial conditions $\dot{x}(0) = \dot{x}_0, \dot{z}(0) = \dot{z}_0$ into account, we get

$$\dot{x} = -2nz + 2nz_0 + \dot{x}_0$$

We insert this result into the third Hill equation, getting

$$\ddot{z} = 2n\dot{x} + 3n^2 z = -n^2[z - (4z_0 + 2x_{0n})]$$

This, too, is the equation of a harmonic oscillator for the expression $z-(4z_0 + 2x_{0n})$, yielding

$$z - (4z_0 + 2x_{0n}) = z_{0n}\sin nt - (3z_0 + 2x_{0n})\cos nt$$

under consideration of the initial conditions $z(0) = z_0, \dot{z}(0) = \dot{z}_0$. We solve for z and find

$$z = 4z_0 + 2x_{0n} + z_{0n}\sin nt - (3z_0 + 2x_{0n})\cos nt$$

Inserting this into the above equation $\dot{x} = -2nz + 2nz_0 + \dot{x}_0$, we get

$$\dot{x} = -(6z_0 + 3x_{0n})n - 2\dot{z}_0\sin nt + (6nz_0 + 4\dot{x}_0)\cos nt$$

This can be integrated directly to deliver with initial condition $x(0) = x_0$

$$x = x_0 - 2z_{0n} - (6z_0 + 3x_{0n})nt + 2z_{0n}\cos nt + (6z_0 + 4x_{0n})\sin nt$$

We summarize the results as

$$\underbrace{\begin{pmatrix} x \\ z \\ \dot{x} \\ \dot{z} \end{pmatrix}}_{\text{final state vector}} = \underbrace{\begin{bmatrix} 1 & 6(\sin nt - nt) & (4\sin nt)/n - 3t & 2(\cos nt - 1)/n \\ 0 & 4 - 3\cos nt & 2(1-\cos nt)/n & (\sin nt)/n \\ 0 & 6n(\cos nt - 1) & 4\cos nt - 3 & -2\sin nt \\ 0 & 3n\sin nt & 2\sin nt & \cos nt \end{bmatrix}}_{\text{time-evolution matrix}} \underbrace{\begin{pmatrix} x_0 \\ z_0 \\ \dot{x}_0 \\ \dot{z}_0 \end{pmatrix}}_{\text{initial state vector}} \tag{8.5.6}$$

and

$$\boxed{\begin{pmatrix} y \\ \dot{y} \end{pmatrix} = \begin{bmatrix} \cos nt & (\sin nt)/n \\ -n \sin nt & \cos nt \end{bmatrix} \begin{pmatrix} y_0 \\ \dot{y}_0 \end{pmatrix}} \tag{8.5.7}$$

These are the basic equations for orbital motion in the vicinity of the reference object and with respect to its co-moving topocentric reference system RSW.

Application to Orbital Rendezvous

A typical application of Eq. (8.5.6) is the design of an orbital rendezvous. If at time $t_0 = 0$ a S/C is at an initial point $r_0 = (x_0, y_0, z_0)$, the problem to solve is: What should be the initial velocity $v_0 = (\dot{x}_0, \dot{y}_0, \dot{z}_0)$ to meet after time t a given target point $r = (x, y, z) = (0, 0, 0)$? The solution can be derived from the equations for x, y, and z of Eqs. (8.5.6) and Eq. (8.5.7) by setting $x = y = z = 0$ and solving for $\dot{x}_0, \dot{y}_0, \dot{z}_0$. If this is done, one straightforwardly obtains

$$\begin{aligned} \dot{x}_0 &= \frac{-2x_0 n(1-\cos nt) + z_0 n(4 \sin nt - 3nt \cos nt)}{3nt \sin nt - 8(1-\cos nt)} \\ \dot{z}_0 &= \frac{x_0 n \sin nt - z_0 n[6nt \sin nt - 14(1-\cos nt)]}{3nt \sin nt - 8(1-\cos nt)} \\ \dot{y}_0 &= -\frac{y_0 \omega}{\tan nt} \end{aligned} \tag{8.5.8}$$

The required delta-v for these maneuvers then is given by

$$\Delta v = \sqrt{(\dot{x}_0 - \dot{x}_{0-})^2 + (\dot{y}_0 - \dot{y}_{0-})^2 + (\dot{z}_0 - \dot{z}_{0-})^2} \tag{8.5.9}$$

where $v_{0-} = (\dot{x}_{0-}, \dot{y}_{0-}, \dot{z}_{0-})$ is the velocity of the S/C just before the impulse maneuver at (x_0, y_0, z_0).

It is an easy exercise to show that in the limit $t \to 0$ Eqs. (8.5.8) pass over into

$$\begin{aligned} \dot{x}_0 &= -\frac{x_0}{t} - nz_0 - \frac{1}{6} n^2 x_0 t + O(n^3 z_0 t^2) \\ \dot{z}_0 &= -\frac{z_0}{t} + nx_0 - \frac{5}{6} n^2 z_0 t + O(n^3 x_0 t^2) \quad @\ t \to 0 \\ \dot{y}_0 &= -\frac{y_0}{t} + \frac{1}{3} n^2 y_0 t + O(n^4 y_0 t^3) \end{aligned}$$

Therefore, for $(nt)^2 \ll 1$, which implies roughly $t < 0.02 \cdot T$, we can write

$$\boxed{\begin{aligned} \dot{x}_0 &= -\frac{x_0}{t} - nz_0 \\ \dot{z}_0 &= -\frac{z_0}{t} + nx_0 \\ \dot{y}_0 &= -\frac{y_0}{t} \end{aligned}} \quad @\ (nt)^2 \ll 1 \tag{8.5.10}$$

These expressions will later be useful to explore maneuvers in the vicinity of the target object.

8.5.3 Flyaround Trajectories

To fly in a controlled way in the vicinity of a target object, we need to know: What does a flyaround trajectory of a S/C look like? We will now explore the two different types of trajectories because they are essential for understanding the general behavior of such a S/C.

The Prolate Cycloid

On November 18, 2008, the astronaut Heidemarie Stefanyshyn-Piper lost her toolbox in space when carrying out repair work outside the International Space Station. She accidentally and gently touched the toolbox (which should have been secured by a line either to her or the ISS, but was not), giving the box a push such that it slowly drifted away from the station (see Figure 8.20).

This accident is a good example to study the trajectory of slowly moving objects near a reference system, which for our purposes is the ISS at an average altitude of 350 km. So, what was the trajectory of the toolbox? It is important to know in which direction the push was relative to the flight direction of the ISS. Because we do not know, we will assume two different situations. First, Heidemarie pushed the toolbox backward, against flight direction, with an initial velocity of, say, $v_0 = (\dot{x}_0, \dot{y}_0, \dot{z}_0) = (-0.1, 0, 0)\ \mathrm{m\,s^{-1}}$. We study the trajectory in the RSW reference system of the ISS, in the center of which the toolbox was lost, so $r_0 = (x_0, y_0, z_0) = (0, 0, 0)$. Under these initial assumptions, we read from Eq. (8.5.6)

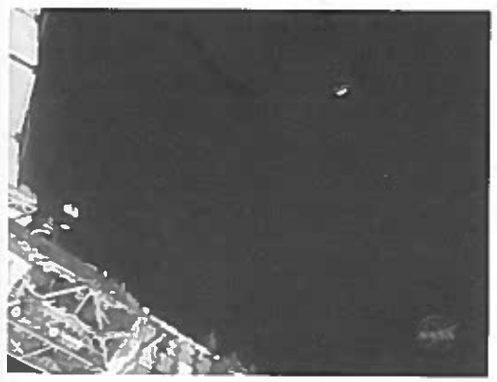

Figure 8.20 The toolbox (top right) of astronaut Stefanyshyn-Piper slowly drifting away from the truss structure of the ISS (bottom left).

$$
\begin{aligned}
x(t) &= \frac{v_0}{n}(4\sin nt - 3nt) \approx v_0 t \\
\dot{x}(t) &= v_0(4\cos nt - 3) \\
z(t) &= 2\frac{v_0}{n}(1-\cos nt) \approx n v_0 t^2 \\
\dot{z}(t) &= 2v_0 \sin nt
\end{aligned}
\tag{8.5.11}
$$

where the approximations are for early times on the trajectory, $nt \ll 1$. If we solve the approximation for x and insert it in the approximation for z, we obtain a parabolic trajectory.

$$z = \frac{nx^2}{v_0}$$

Because v_0 is negative, we get a down curved parabola: The toolbox dives below the orbit of the ISS (see Figure 8.21), which first seems to be quite surprising. Interestingly, the toolbox comes to a halt in $-x$-direction when $\cos nt = 3/4$ and thereafter moves back toward the ISS, yet at increasingly lower altitudes. After half an orbit, it reaches the lowest point (perigee), and then it climbs up to reach the initial altitude of 350 km after a full revolution of the ISS, however, at a distance of 1.65 km in front of the ISS. The toolbox will repeat this loopy motion indefinitely, thereby moving away from the ISS—the toolbox will be lost. Such a winded trajectory is mathematically called a *prolate cycloid*.

What is the reason for such a weird trajectory? When the toolbox is kicked off backward, it has a lower velocity as it should have for a circular orbit at this altitude. So the centrifugal force, $F_c = mv^2/r$, is lower than the gravitational force, which rapidly pulls the box down. But upon dropping it gains speed, which brings it to a lateral halt at 42 m away from the ISS. With increasing speed, the centrifugal force increases that after half a revolution at perigee brings the decline to a halt at 350 m below and 824 m ahead of the ISS. Since the speed now is too large for this altitude, the box dives up and decelerates until it "kisses" the orbit to iterate its dive. The size of the cycloid depends linearly on the initial velocity, while its orientation reverses when v_0 is with or against the flight direction of the ISS. Figure 8.22 gives an overview of this behavior for different initial x_0.

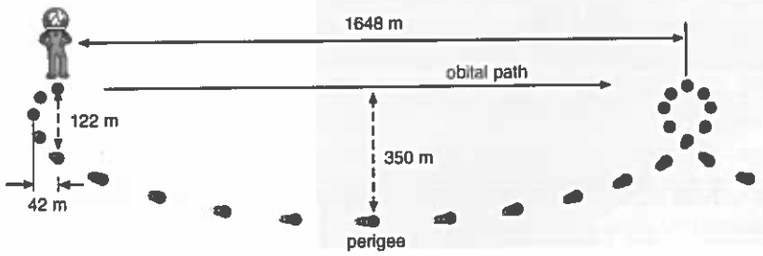

Figure 8.21 The prolate cycloid trajectory of the toolbox that Heidemarie lost, if its initial motion $v_0 = -0.1\ \mathrm{m\,s^{-1}}$ was reverse to the flight direction of the ISS. ISS altitude is $h = 350$ km.

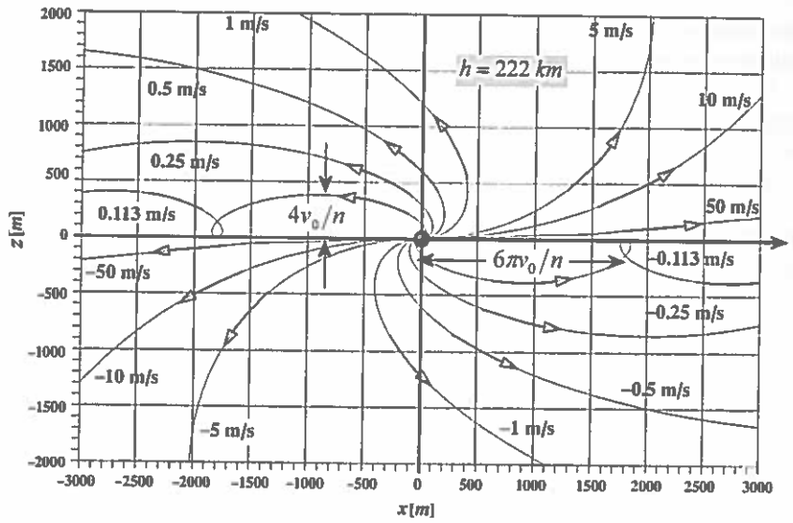

Figure 8.22 Shown are for different v_0 in x direction the trajectories (prolate cycloid) of the object moving relative to a reference point (center dot, which itself moves on an orbit at altitude $h = 222$ km to the right (bold arrow)).

The reason for this weird motion can be understood when seen in the geocentric reference system (see Figure 8.23). An object initially slower than the ISS at point 0 will have less orbital energy and hence move on an elliptic trajectory with smaller major-axis than the ISS. This implies that the object will drop below the ISS and will have a smaller orbital period, so showing up in front of the ISS after one revolution at

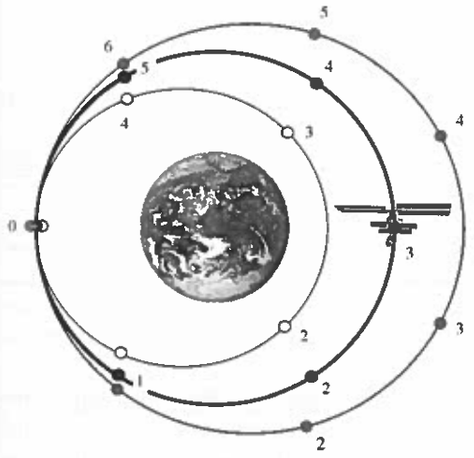

Figure 8.23 A schematic sketch of the prolate cycloid motion as viewed from the inertial reference frame of Earth. The smaller ellipse is for an object with smaller velocity and the larger ellipse with a larger velocity at point 0. The numbered points give the positions on each orbit after constant time intervals.

the initial point 0. An object with a larger initial velocity will move on a larger ellipse with reversed behavior.

This view in an inertial reference frame makes clear that the prolate cycloid is the trajectory of a Hohmann transfer as observed in the target's reference frame. This should have been clear from the very beginning, because the initial kick-burn is tangential to the initial orbit. This is the attribute of a Hohmann transfer.

The Ellipse

We now assume that Heidemarie pushed the toolbox upward, vertically to the flight direction, with the same initial velocity $v_0 = (\dot{x}_0, \dot{y}_0, \dot{z}_0) = (0, 0, 0.1)\,\mathrm{m\,s^{-1}}$. Interestingly, the trajectory of the toolbox would be totally different. From Eq. (8.5.6), we derive the trajectory to be

$$\begin{aligned} x &= 2\frac{v_0}{n}(\cos nt - 1) \approx -nv_0t^2 \\ z &= \frac{v_0}{n}\sin nt \approx v_0 t \end{aligned} \tag{8.5.12}$$

again with approximations for early times on the trajectory, $nt \ll 1$. By removing the time parameter for $nt \ll 1$, we again find a parabola that, however, opens to the rear side of the ISS.

$$z = \sqrt{-\frac{v_0}{n}x}$$

To derive the full trajectory, we recognize that we can solve both equations for $\cos nt$ and $\sin nt$ and via the trigonometric equation $\sin^2 x + \cos^2 x = 1$, we find

$$\frac{(x + 2v_0/n)^2}{(2v_0/n)^2} + \frac{z^2}{(v_0/n)^2} = 1$$

which is the equation of an ellipse with semi-major axis $a = 2v_0/n$ along the x-axis and semi-minor axis $b = v_0/n$ along the z-axis, and therefore eccentricity $e = \sqrt{1 - b^2/a^2} = \sqrt{3/4} = 0.8660\ldots$. For varying initial velocities, details of such ellipses are shown in Figures 8.24 and 8.25.

We can summarize the behavior of the toolbox as follows: When initially moving up, the orbital velocity remains constant. However, the angular frequency $\omega = v/r$ and the centrifugal force $F_c = mv^2/r$ decrease. Owing to this, the toolbox falls behind the ISS and also loses vertical speed, because the gravitation pull becomes bigger than the centrifugal force. After a quarter of an orbital revolution of the ISS, the toolbox drops down and crosses the orbit after half an orbital revolution, but now with downward velocity. The inverse behavior thereafter would bring the toolbox back to Heidemarie.

If a S/C relative to a target object starts its trajectory from the orbital path of the target object and initially moves along the x or z direction, the ellipse and the prolate cycloid are the two possible forms of this trajectory. The trajectories become more intricate if v_0 is not pointing into the x or z direction, and the initial location is displaced from the orbital path. In any of these cases, the main features of such

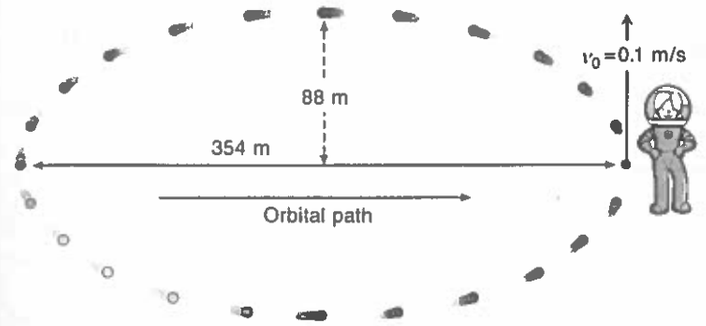

Figure 8.24 The path of Heidemarie's toolbox if pushed with 0.1 m s^{-1} along the positive z direction. The box follows a closed elliptical path and returns to Heidemarie after one orbital revolution of the ISS. ISS altitude is $h = 350$ km.

convoluted trajectories are the ellipse and the prolate cycloid. The reason is, whatever the initial conditions of the S/C might be, it will move on an ellipse around the Earth. If its semi-major axis a is the same as that of the target object, it will just fly around the target object periodically. If its a is different, its orbital period will be different, and therefore the periodic motion will be superimposed by a motion that let the S/C and the target object drift relative to each other. These two features are extensively used for applied orbital rendezvous maneuvers to which we will turn now.

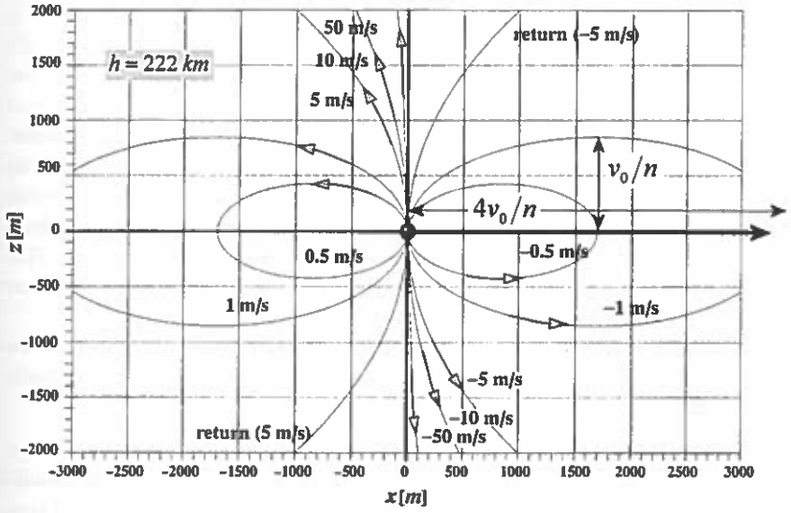

Figure 8.25 Shown are the trajectories (ellipses) of the object moving relative to a reference point (center dot, which itself moves on an orbit at altitude $h = 222$ km to the right (bold arrow)) for different v_0 in z direction.

8.6 Orbital Rendezvous

Rendezvous and docking (R&D) form some of the most complex maneuvers to be carried out by a spacecraft in spaceflight. In order to accomplish successful rendezvous and mating of two spacecraft, absolute and relative navigation on orbit, sensing of the target object, precise attitude determination and control, maneuver planning, and the use of highly complex mechanisms must be mastered. The development of these skills was the purpose of the US Gemini program and the early Soviet Soyuz program, and they were further refined in the era of the Space Shuttle and the ISS. In recent years, the desire for autonomous robotic on-orbit servicing systems and plans for more ambitious human and robotic exploration of the solar system create new challenges for technology and mission designers.

The purpose of any R&D mission is to establish physical contact between two or more spacecraft to establish electrical, material, and crew exchange. Therefore, R&D is a prerequisite for the construction and maintenance of space stations such as the ISS, as well as any servicing mission to satellites in Earth orbit. Such missions can be manned (e.g., the Hubble servicing missions) or unmanned (e.g., future On-Orbit Servicing). R&D is also a mission-enabling skill in human and robotic exploration of the solar system. Without successful R&D, the Apollo missions would not have been possible.

As the established term *rendezvous and docking* implies, the involved operations are divided into two distinct parts, each with a particular set of goals.

Rendezvous: During the rendezvous part of the mission, the involved spacecraft are guided to meet in the same volume of space at the same time. In most applications, the target object (also often referred to as *resident space object*) is inert, and the interceptor (a.k.a. chaser) performs all maneuvers to meet the position and time requirements. However, as an exception to this rule, in the so-called *control box rendezvous*, it is the target spacecraft that executes a number of maneuvers to meet the interceptor after it was launched. This reduces interceptor vehicle propellant consumption, naturally at a cost to the target. It therefore can only be performed with targets having orbit maneuvering capabilities, which usually rules out space stations and a large number of satellites. Nonetheless, this type of rendezvous was performed on some Space Shuttle missions (e.g., STS-49 to service Intelsat VI) and was also planned for the contingency rescue mission STS-400 to Atlantis' Hubble Servicing Mission 4.

Docking: The goal of docking in a mission is to establish physical contact between the involved spacecraft. Although commonly the term *docking* is used, there actually exist two distinct cases: *docking*, and *capture and berthing*.

1) *Docking.* The interceptor approaches the target with non-zero relative velocity, brings its docking tool into alignment with the target's counterpart, and establishes a firm structural connection by using its own momentum. Docking therefore relies only on maneuvering capabilities of the two spacecraft and on properly functional docking tools. This approach was used during Gemini and Apollo and still is in use with Soyuz/Progress, the Space Shuttle, and ESA's Automated Transfer Vehicle (ATV) missions to ISS.
2) *Capture and berthing.* The interceptor is maneuvered into close proximity of the target and an initial mechanical connection between both is established by a robotic manipulator. This manipulator can be situated on the interceptor (as is the case with the Shuttle Robotic Manipulator System (RMS) used for capturing the Hubble Space Telescope) or on the target vehicle. This is the approach taken with the Space Station Remote Manipulator System (SSRMS) on ISS capturing the Japanese H-II Transfer Vehicle (HTV). After capture, the captured spacecraft is then moved by the manipulator to a berthing position, which is a device similar to a docking port.

   The choice of the manipulator's location is, on the one hand, dependent on the sizes and masses of the spacecraft. The attitude of a heavier spacecraft is less influenced by the disturbance torques caused by the movement of the manipulator. On the other hand, a space manipulator is a very complex and hence an expensive mechanism. It will therefore be mounted on the spacecraft with the longer lifetime and/or reentry capability, and not on the disposable spacecraft like HTV.

The combination of both rendezvous and docking is not an end to itself, but serves to fulfill the purpose of a mission. It therefore must always be carefully planned and designed within the larger mission context. This influences not only design decisions such as launch windows, approach trajectories, and the selection of sensors, but also the general approach modes, be it operator-in-the-loop or autonomous robotic. To understand the challenges, choices, and trade-offs involved, the following section provides details about R&D mission design.

Mission Phases

Generally, R&D missions involve both an interceptor spacecraft, which begins the mission on the launch pad, and a target spacecraft, which is usually already in orbit by the time of the interceptor's launch. The following sections will discuss the mission phases of typical R&D missions in LEO, which are in the following order:

1) Launch
2) Phasing
3) Homing
4) Closing
5) Final Approach
6) Docking/Capture.

This sequence of mission steps results in a typical R&D mission profile as shown in Figure 8.26.

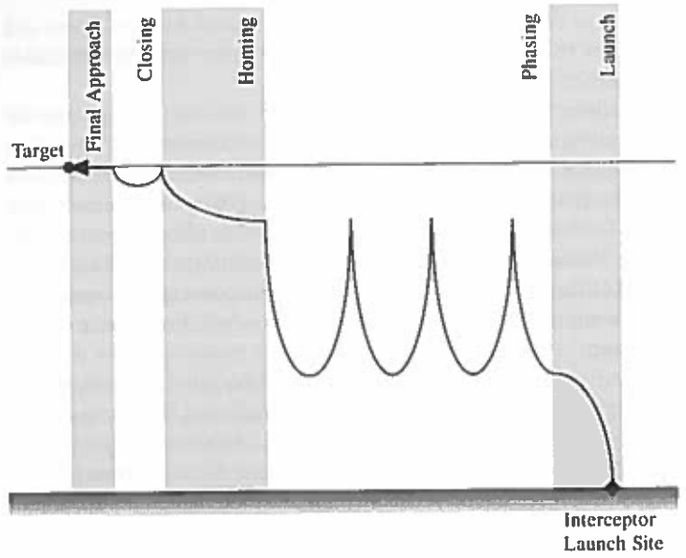

Figure 8.26 Sketch of a typical R&D mission profile consisting of launch phase, phasing maneuvers, homing, and close range rendezvous (closing and final approach) including docking.

8.6.1 Launch Phase

The launch phase comprises the injection of the interceptor into the orbital plane of the target, as well as achieving stable orbital conditions. To directly meet the plane of the target, the interceptor must be launched inside a narrow launch window. This launch window is derived in the following steps.

First, we derive the launch azimuth φ, which is the angle between the launch trajectory and the geographic North, i.e., the local direction in which to launch. If we denote the target's orbit inclination as i and the launch site latitude as β, we have from Figure 8.27 and according to Napier's rules for spherical angles $\cos i = \cos\beta \cdot \sin(180^\circ - \varphi) = \cos\beta \cdot \sin\varphi$, from which we obtain the following two solutions:

$$\begin{aligned} \varphi_1 &= \arcsin\frac{\cos i}{\cos\beta} && @\ \textbf{ascending pass} \\ \varphi_2 &= 180^\circ - \arcsin\frac{\cos i}{\cos\beta} && @\ \textbf{descending pass} \end{aligned} \tag{8.6.1}$$

The reason is, a launch site passes twice a day through a given orbital plane: Once on the ascending pass of the target orbit with launch azimuth φ_1, the other on the descending pass with launch azimuth φ_2. So, if for a launch site the launch azimuth is not limited, there are two launch opportunities every day.

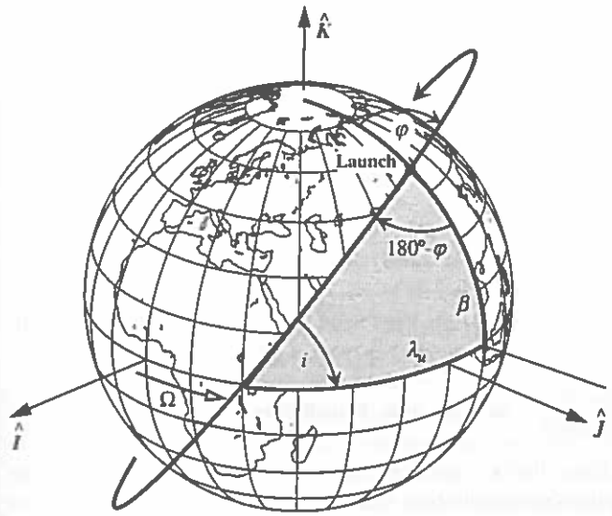

Figure 8.27 Launch window trigonometry. Illustrated are the target orbit with RAAN Ω and inclination i, launch site latitude β, launch azimuth φ, and auxiliary angle λ_u.

From $\cos i = \cos\beta \cdot \sin\varphi$, we can read that because $|\sin\varphi| \leq 1$, we have $\cos i \leq \cos\beta$, implying $i \geq \beta$. So there exists no launch azimuth to achieve an $i < \beta$, or in other words: Orbits with $i < \beta$ cannot be reached directly. This seemingly paradoxical situation is elucidated in Figure 8.28. For example, launchers from

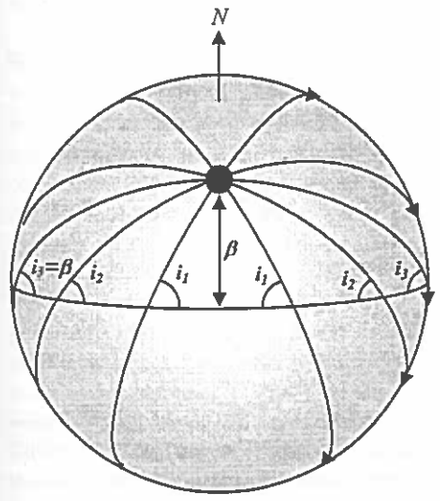

Figure 8.28 Whatever the launch azimuth is, the accessible orbit inclination i is always larger than the latitude of the launch site β. If the launch azimuth is $\varphi = 90^\circ$, then $i = \beta$ is achieved.

Kennedy Space Center with $\beta = 28.47°$ cannot reach orbits with $i < 28.47°$. Only in the limiting case $\varphi = 90°, 270°$, i.e., if the launch azimuth is East or West (into a retrograde orbit), we obtain $i = \beta$. If orbits $i < \beta$ need to be reached, the launcher is first launched with $i = \beta$. When its orbit intersects the desired target orbit having $i < \beta$, a plane change maneuver (a.k.a. dogleg maneuver) is performed that, however, is associated with large propellant consumption and thus reduced payload for a given target orbit.

What is the right time to launch? The Universal Time of launch, T_{UT}, defines the moment in time when the launch site is in the plane of the International Space Station's orbit, the so-called *in-plane time*. At this launch time, the interceptor reaches the targeted orbital plane with the least effort (delta-v budget). It is given by

$$T_{UT} = \frac{\theta_{GMST} - \theta_{GMST0}}{\omega_{\oplus}} \qquad \textbf{in-plane time (launch time)} \qquad (8.6.2)$$

where $\omega_{\oplus} = 7.2921150 \times 10^{-5}\ s^{-1}$ is Earth's sidereal rotation rate. The hour angle θ_{GMST}, representing the Greenwich Mean Sidereal Time (GMST) for the launch to occur at, is calculated as

$$\theta_{GMST} = \Omega + \lambda_u - \lambda$$

where the auxiliary angle λ_u (see Figure 8.27), which is the difference between the launch site longitude λ and the target orbit's RAAN Ω, is calculated from Napier's rules as

$$\lambda_u = \arccos\frac{\cos\varphi_{1,2}}{\sin i} = \pm\arcsin\frac{\sqrt{1-(\cos i/\cos\beta)^2}}{\sin i}$$

The required hour angle θ_{GMST0} of a particular launch day at 00:00 h can be obtained from the Astronomical Almanac of the given year or from

$$\theta_{GMST0} = 100.4606184° + 3600.77005361°\ s^{-1} \cdot T_{UT1} + 0.00038793°\ s^{-2} \cdot T_{UT1}^2 - 2.6 \times 10^{-8}°\ s^{-3} \cdot T_{UT1}^3$$

The term T_{UT1} denotes the number of *Julian centuries* of the launch day at 00:00:00 h elapsed since the *standard epoch* J2000, which is given as

$$T_{UT1} = \frac{JD - 2\,451\,545.0}{36\,525}$$

where in turn the Julian date JD of the given launch day at 00:00:00 h, which should be provided in terms of years $\langle yyyy \rangle$, months $\langle mm \rangle$, and days $\langle dd \rangle$, is computed by

$$JD = 367 \cdot \langle yyyy \rangle - INT\left\{1.75 \cdot \left[\langle yyyy \rangle + INT\left(\frac{\langle mm \rangle + 9}{12}\right)\right]\right\} + INT\left(\frac{275}{9}\langle mm \rangle\right) + \langle dd \rangle + 1\,721\,013.5$$

where the function $INT(x)$ truncates the real number x to the next lower integer number.

Launch Windows

Any deviation from the in-plane launch time would implicate a dogleg maneuver and hence an additional propulsion demand for a plane change maneuver (see Eq. (8.1.2) and Figure 8.2 for details). On the other hand, since this precision is impractical to achieve both for organizational and technical reasons, one allows a small amount of time for the launch of the interceptor on both sides of the ideal launch time T_{UT}. This is the so-called **planar launch window**. The width of the planar launch window depends on the launch azimuth. If the launch azimuth is $\varphi \approx 90°$, i.e., if the inclination matches the launch site latitude, the launch window is typically up to 1 h because no later plane adjustment would be necessary. With decreasing launch azimuth, any deviation of the launch time from the in-plane time will cause increasing plane differences and hence an increasing propulsion demand to correct them. For Shuttle launches to the ISS ($i = 51.6°$), the planar launch window decreases to only 10 min. Targets above 57° inclinations have planar launch windows of less than 5 min. In missions to ISS, in practice the Shuttle launch time is appointed to the opening of the launch window, i.e., 5 min before the in-plane time. In case of a launch delay due to a possible countdown problem, there remain 10 min to fix the problem. If no problem occurs, the Shuttle is put on hold for 5 min and is launched on in-plane time.

Apart from orbital mechanics, there are other restrictions defining other kinds of launch windows on different time scales. An important consideration is the *sun angle*, which is the angle between the direction to the Sun and the targeted orbital plane. The sun angle is important for visibility conditions during final approach (cf. Figure 8.38 where the Shuttle needs to see the ISS during daytime conditions, in particular during final approach) and for solar power generation of the docked spacecraft. For the Space Shuttle, another concern is the ability to monitor its ascent and to visually check the external tank for damages during launch and ascent.

When launching toward ISS, traffic conditions also impact launch window planning, since multiple spacecraft such as Soyuz, Progress, ATV, HTV, or Shuttle want to approach the station during beneficial lighting conditions. All these factors must be considered in mission planning, which leads to the small number of launch windows available to ISS or Hubble per year. This is the reason why the failure to launch a mission during the originally intended window can cause launch delays of months, instead of hours or days as dictated by orbital mechanics. Also, the so-called *phase window* (see next section) restricts the launch opportunities.

For a given launch site, the range of permitted launch azimuths is usually restricted due to safety concerns of flying a launch vehicle over densely populated areas. For instance, the launch azimuth restrictions at Kennedy Space Center are $35^\circ \leq \varphi \leq 120^\circ$, where the lower bound is due to the US West Coast and the upper bound to the Caribbean islands. This restricts the Shuttle to have only one launch opportunity per day to the ISS.

8.6.2 Phasing

After successful completion of the launch phase, the interceptor spacecraft achieves a stable orbit within the same plane as the target. The two orbits are thus coplanar and typically near circular. (Alternatively, the interceptor is in a plane from which the target plane can be reached within the capabilities of the orbital maneuvering system of the interceptor.)

However, the target might be anywhere on its orbit. Therefore, the first part of the target rendezvous, the so-called *far range rendezvous*, requires first a reduction in the distance to the target, until it can be acquired by the sensors of the interceptor, and then a transfer to a stable holding point on the trailing side of the target.

This first part of far range rendezvous phase is called *phasing* because it is to reduce the so-called *(orbital) phase angle* ϑ, which is the difference in true anomaly as measured in the flight direction from the target to the interceptor. Phasing is typically conducted in absolute navigation, i.e., with reference to an inertial reference frame, and guided by ground control. As an example, Space Shuttle phasing maneuvers are planned by mission control using orbit determination data obtained by ground radar and *Tracking and Data Relay Satellite System* (TDRSS) Doppler measurements. By processing both the target and interceptor tracking data, the orbital phase angle is determined.

Usually, the interceptor needs to chase the target, so only negative initial phase angles are permitted. This is why the interceptor is often called *chaser*. In addition, only certain initial phase angles are permitted. Owing to performance limitations and constrained crew activities, this so-called **phase window** (window accounting for phase angle makeup capability) varies for the Shuttle between $40^\circ \leq -\vartheta_i \leq 360^\circ$. The relationship of the phase window to the planar launch window changes each day and depends on the target's orbital period and inclination.

Owing to a given initial phase angle to be made up, the interceptor will have finalized its launch trajectory on a generally slightly elliptic or circular orbit with its semi-major axis a_I smaller than the a_T of the target orbit. Whether the initial apogee coincides with the target orbit depends on the particular rendezvous strategy, but usually the interceptor orbit nowhere crosses the target orbit. Because $a_I < a_T$, the mean orbital frequency (mean motion) is larger than that of the target, which implies that the orbital phase angle is reduced continuously—the goal of phasing.

How much is the phase angle reduced in course of one orbital revolution? Assuming small differences in the semi-major axes, which is a quite good

approximation for LEO and since $n = \sqrt{\mu/a^3} = 2\pi/T$ of the target, the phase reduction after one orbital revolution is

$$\Delta\vartheta = \Delta n \cdot T = \left(\frac{dn}{da} \cdot \Delta a\right) \cdot T = -\frac{3}{2}\frac{n}{a} \cdot \Delta a \cdot T$$

Therefore,

$$\Delta\vartheta = -3\pi\frac{\Delta a}{a} \quad \text{per orbit} \tag{8.6.3}$$

The minus sign reflects the fact that the phase angle from the target to the interceptor decreases if $a_I > a_T$, i.e., if $\Delta a > 0$. This phase angle reduction relates to a closing distance of

$$\Delta x = \Delta\vartheta \cdot a = -3\pi \cdot \Delta a \quad \text{per orbit}$$

To give an example, the ISS orbits Earth at an altitude of about $h = 350$ km. Owing to drag becoming too excessive, the lowest chaser altitude is limited to about $h = 200$ km. This implies $\Delta a \geq -150$ km. So, the Shuttle is able to approach the ISS maximally with $\Delta\vartheta \leq 12^\circ$ per orbit equaling $\Delta x \leq 1400$ km per orbit. If the ISS, in the worst case, has an initial orbit phase angle of 360°, it will take 2 days to get there.

8.6.3 Homing Phase

The interceptor is now on a phasing orbit about 50 km away from the target, drifting slowly toward the target. The objective of the upcoming homing transfer, the second part of the far range rendezvous, is to transfer the interceptor to a stable holding and aiming point in the vicinity of the target (see Figures 8.26 and 8.29). A prerequisite of the transfer is that the target must be acquired by the relative navigation sensors of the interceptor. For the Space Shuttle, mission control hands over rendezvous guidance to the orbiter's crew at 74 km from the target. At this point, a target like the ISS can be tracked using star trackers or radar.

With the homing maneuver also the relative approach velocity must be reduced to a safe level. In addition, the dispersions in position, orientation, and angular rate must be reduced to meet the conditions required for the upcoming close range rendezvous. This includes the synchronization of the motion timeline of the two spacecraft.

LVLH Reference System

For the discussion of the now following rendezvous approaches, the *Local Vertical Local Horizontal* (LVLH) reference system is defined (see Figure 8.30). The origin of LVLH is located at the center of mass of the target. Its $+x$-axis, also called the + V-bar, points along the target's velocity vector. The $-z$-axis, referred to as + R-bar, points antiparallel to the target's radial vector. The $-y$-axis, also called + H-bar, completes the right-handed system and thus points along orbit normal. In the

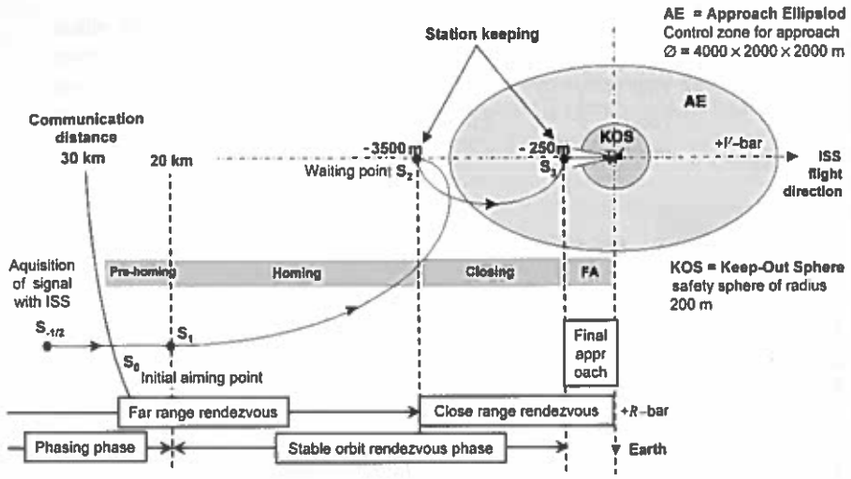

Figure 8.29 Homing, closing, and final approach profile and phases for ISS rendezvous. ISS safe approach procedures require station-keeping points S on the V-bar, an approach corridor, and a Keep-Out Sphere around ISS that approaching spacecraft must use.

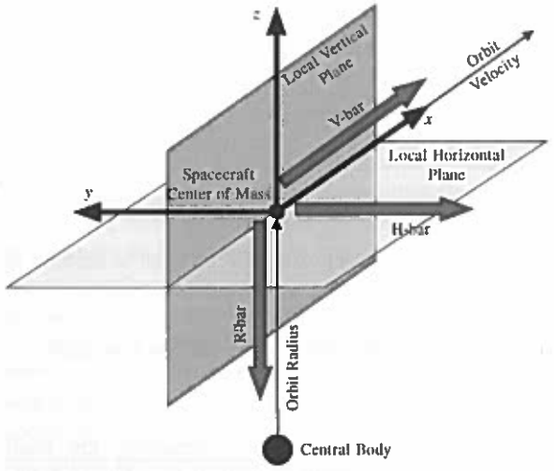

Figure 8.30 Local Vertical Local Horizontal reference system: +V-bar (+x-axis) is in the direction of the spacecraft's velocity vector, +R-bar (+z-axis) is in the direction of the negative radius vector, and +H-bar (−y-axis) completes the right-handed system.

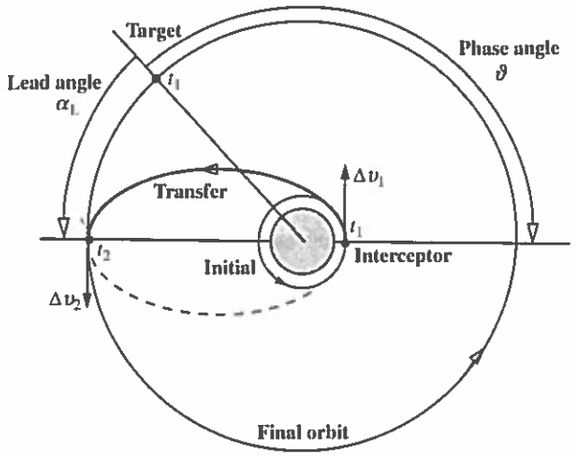

Figure 8.31 General Hohmann transfer of an interceptor to meet a target point in a circular coplanar orbit. At time t_1 the required phase angle is ϑ and the interceptor begins the phasing maneuver by applying the thrust Δv_1. After a half revolution on the transfer orbit, the interceptor reaches the target point at time t_2. The maneuver Δv_2 moves the interceptor onto the target orbit and finalizes the Hohmann transfer.

following, a "+V-bar approach" means that the interceptor approaches the target on the target's +V-bar (into −V-bar direction). Accordingly, a "− R-bar approach" is on the target's −R-bar (into +R-bar direction), etc.

Homing Transfer

The homing transfer, which commences at point S1 in Figure 8.29, is a classical Hohmann transfer as described in Section 8.3. The principle situation is shown in Figure 8.31, where the orbits, however, are not to scale because at the end of the phasing phase, the two orbits with $a \approx 6750$ km in LEO have a radial distance of typically only about 10 km. Owing to this, the phase angle at the beginning of the Hohmann maneuver is practically zero while its complement to 180°, the so-called *lead angle*, is $\alpha_L = 180° - \vartheta \approx 180°$.

Let ϑ_i be the initial phase angle and let ϑ_f be the final phase angle at S2 behind the target. The key question is: At a given a, Δa, and ϑ_f, what is the right ϑ_i and the right tangential kick-burn Δv to get to S2? To find an answer, we apply from Section 8.3.2 the essential results of a Hohmann transfer to adjacent circular orbits as for rendezvous orbits

$$a_H = \frac{1}{2}(a_i + a) = a\left(1 + \frac{\Delta a}{2a}\right)$$

$$t_H = \pi\sqrt{\frac{{a_H}^3}{\mu}}$$

Now, while the interceptor transits over an orbit angle of 180° on the Hohmann transfer orbit, the target with $n = \sqrt{\mu/a^3}$ covers the orbit angle.

$$\Delta\theta = n \cdot t_H = 180^\circ \cdot \left(\frac{a_H}{a}\right)^{3/2} = 180^\circ \cdot \left(1 + \frac{\Delta a}{2a}\right)^{3/2} \approx 180^\circ \cdot \left(1 + \frac{3}{4}\frac{\Delta a}{a}\right)$$

Because in LEO $\Delta a/a \approx 10^{-3}$, we could safely neglect terms of higher order. Therefore, we have for the initial phase angle

$$\vartheta_i = \vartheta_f + (180^\circ - \Delta\theta) = \vartheta_f - 180^\circ \cdot \frac{3}{4}\frac{\Delta a}{a}$$

or

$$\vartheta_i = \vartheta_f - 135^\circ \frac{\Delta a}{a} \tag{8.6.4}$$

For the required delta-v, we find with a circular orbital velocity $v = \sqrt{\mu/a}$

$$\Delta v = v_I - v_T = v_T\left(\sqrt{\frac{a}{a+\Delta a}} - 1\right) = v_T\left(\sqrt{1 - \frac{\Delta a}{a}} - 1\right)$$

from 8.3.7

and hence

$$\Delta v = -\frac{1}{2}\frac{\Delta a}{a}\sqrt{\frac{\mu}{a}} \tag{8.6.5}$$

Taylor (McLaurin) series by $f(x) = f(0) + f'(0)x + \dots$

Example:
The Shuttle shall perform a homing maneuver from $\Delta a = -10$ km to a waiting point $S2 = 3$ km behind the ISS at $h = 350$ km.
We have $\vartheta_f = (180^\circ/\pi) \cdot (10/6728) = 0.085^\circ$ and $v_T = 7.697\ km\ s^{-1}$. With this we get $\vartheta_i = \vartheta_f + 0.201^\circ = 0.286^\circ$. This means the Shuttle has to perform a burn with $\Delta v = 5.72\ m\ s^{-1}$ into flight direction at a position 33.6 km behind the ISS. Because the Shuttle initially is 10 km below the ISS, the viewing distance to the ISS at burn is $\sqrt{10^2 + 33.6^2} = 35.0\ km$

NASA's Space Rendezvous History
At NASA there exist two general approaches for homing and closing maneuvers: The historical *coelliptic rendezvous* and today's *stable orbit rendezvous* (SOR).

Coelliptic Rendezvous
Coelliptic orbits are coplanar elliptic (including circular) orbits with a common occupied focus (see Figure 8.32). The arguments of perigee ω are equal, meaning that the lines of apsides of the orbits are congruent. In addition to this, the differences in perigee and apogee radii are equal. In a spacecraft-fixed reference frame, coelliptic orbits appear as two parallel lines. These particular orbits allow easy, intuitive, and robust maneuver planning by means of the so-called *trigger angle targeting*. This technique was developed during the Gemini program. It allows astronaut pilots to reliably achieve rendezvous by pointing the interceptor spacecraft at the target at a certain trigger angle τ (see Figure 8.32) relative to the direction of flight and then engaging the orbital maneuvering thrusters, the so-called *Terminal Phase Initiation* (TPI). The trigger angle can be measured with simple cueing devices similar to a sextant. During the transfer, the target will move along its orbit within the so-called *transfer angle* α (the orbit angle covered during transfer). If rendezvous is achieved within a single revolution of the target, thus with $\alpha < 360^\circ$, it is called a *direct rendezvous*. Any case with multiple target revolutions is referred to as *indirect rendezvous*. The point aimed at by the interceptor, in front of or behind the target, is referred to as the *downrange targeting location*.

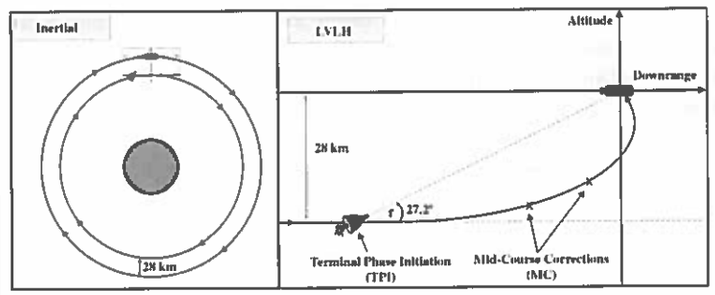

Figure 8.32 Gemini coelliptic rendezvous in inertial and spacecraft reference frames; τ denotes the trigger angle between the direction to the target and the local horizontal plane at which the transfer maneuver is triggered.

It can be shown (see Woffinden (2007)), and this is a key property of coelliptic rendezvous, that for direct rendezvous, the elevation trigger angle τ is independent of the angular frequency ω and the relative altitude of the coelliptic trajectory. Hence, the same trigger angle applies for all orbits, regardless of the coelliptic height differential. For indirect rendezvous, the trigger angles show dependency on the ratio between the downrange targeting location and the relative altitude of the coelliptic trajectory. In recent numerical simulations, it was determined that the optimal trigger angle for a minimum Δv intercept maneuver is 27.0°, with a transfer angle of 163.1°. Interestingly, this is not equal to a Hohmann transfer with a triggerangle of 0° and a transfer angle of 180°. In reality, this optimal angle will not be perfectly achievable. A range between 26.8° and 27.3° was therefore identified as providing optimal combinations of required Δv, line-of-sight (LOS) approach rates, and positioning accuracy.

Interestingly, without running numerical computer simulations, NASA selected a trigger angle of 27° with a transfer angle of 130° for Gemini/Apollo rendezvous operations. For these manned rendezvous missions, trigger angle targeting was particularly attractive. It allowed the use of the astronauts' eyes and simple elevation cueing for maneuver triggering in case of the failure of the rendezvous radar system. After applying the initial Δv along LOS, the pilot performed one or two midcourse correction maneuvers, before finally approaching the target for docking. During final approach, the pilot benefited from a low inertial LOS approach rate during final breaking and approach, as well as from good visibility of the target against the star background. This was important since LOS closing rates are difficult to judge visually without ambient references.

Coelliptic rendezvous remained NASA's rendezvous approach of choice throughout Gemini and Apollo. Its major strength was the backup capability to perform the TPI burn manually. It was then modified into a *dual coelliptic rendezvous* profile for the Skylab missions. In this profile, the interceptor flew a coelliptic transfer onto a holding orbit below the target. From there another coelliptic maneuver finalized rendezvous. The modifications were applied to improve the final approach lighting conditions for manual piloting, as well as the quality of long-range optical tracking using reflected sunlight. This dual coelliptic profile was then also the baseline for Shuttle R&D missions. Given the characteristics of typical Shuttle rendezvous targets, there existed concerns regarding the usability and quality of optical tracking of small target objects using reflected sunlight in the presence of Earth's illuminated surface and bright celestial objects. Another issue was the depletion of the Shuttle's *Reaction Control System* (RCS) propellant due to high relative approach velocities. This initially led to the adoption of a so-called *tuned coelliptic rendezvous* (TCR) profile.

Stable Orbit Rendezvous

For current space station operations, all these coelliptic rendezvous approaches were replaced by the so-called *stable orbit rendezvous*. Such a SOR was first flown on Gemini XI and was later suggested to address the concerns over target tracking and propellant consumption for Space Shuttle R&D. The reason is that it supports inertial approaches with lower relative velocity than the inertial approaches from the Apollo legacy coelliptic profile. In addition, a stable orbit profile desensitizes the mission timeline from trajectory considerations, as the interceptor could theoretically remain at the waiting point for indefinite periods of time. Stable orbit station-keeping at multiple kilometers of distance to the target (15 km for Space Shuttle ISS approaches) was also preferable to the close range (at distances of tens of meters) station-keeping associated with coelliptic approaches. In such close proximity, continuous crew monitoring and frequent correction maneuver are needed, resulting in high propellant expenditure. Therefore, the advantages of SOR profiles over coelliptic approaches are lower propellant consumption and

stable station-keeping points on V-bar, leading to less demand on crew position monitoring and correction. Hence, the SOR has become the standard for ISS operations for Space Shuttle, Soyuz, and ATV, as well as for other rendezvous operations, such as with the Hubble Space Telescope.

For more details on coelliptic and Space Shuttle R&D missions, refer to Goodman (2006).

8.6.4 Closing Phase

Once on the target orbit at S2 (see Figure 8.29), jets are fired to bring the interceptor to a hold at a safe distance about 3 km behind the target. The target now is within range of the interceptor sensors, and thus relative navigation can commence. This station-keeping point S2 is essential to assess the situation and plan the upcoming closing maneuver.

The closing maneuver depends on the type of final approach: For a final ±R-bar approach, the interceptor needs to get to the ±R-bar below/above the target. For a final +V-bar approach, the interceptor needs to proceed further on the −V-bar closer to the target to the station-keeping point S3, and for a +V-bar approach, the interceptor has to fly around the target to approach it from the leading end. Anyway, with the closing maneuver we ingress the *Approach Ellipsoid* of the ISS. All operations inside the Approach Ellipsoid are "combined operations" involving the mission control authorities in Houston and Moscow. From here on safety as not to collide with the ISS has the highest priority.

−V-bar Approach

Let us assume that the docking port is on the trailing end of the target and therefore an approach further on the −V-bar is favorable. What are the options to carry it out? In Section 8.5.3, we have seen that we may approach the target on the V-bar via a prolate cycloid (which is a Hohmann trajectory; see end of section "Ellipse" in Section 8.5.3) or via an ellipse. The decision is based on safety versus efficiency: If in course of the prolate cycloid we would lose control over the interceptor, we would drift away infinitely and if it is a "flat" cycloid, we might even hit the target. However, if safety is not paramount, then one could traverse the distance from S2 to S3 by one or several cycles keeping the momentum along the V-bar and hence save fuel. At each reversal point, one could even stop the approach, assess the situation, and fine-tune the further approach. This option is chosen by NASA for the Shuttle closing phase (see Figure 8.38). If safety is top priority, then the ellipse trajectory is the choice, because if control over the interceptor would be lost, it would automatically return to S2. However, this method requires to fire the jet at every intersection with the V-bar, thus coming to a halt and thereafter repeat the whole cycle procedure. "Safety-first" requirement, of course, comes at the expense of a higher propulsion demand.

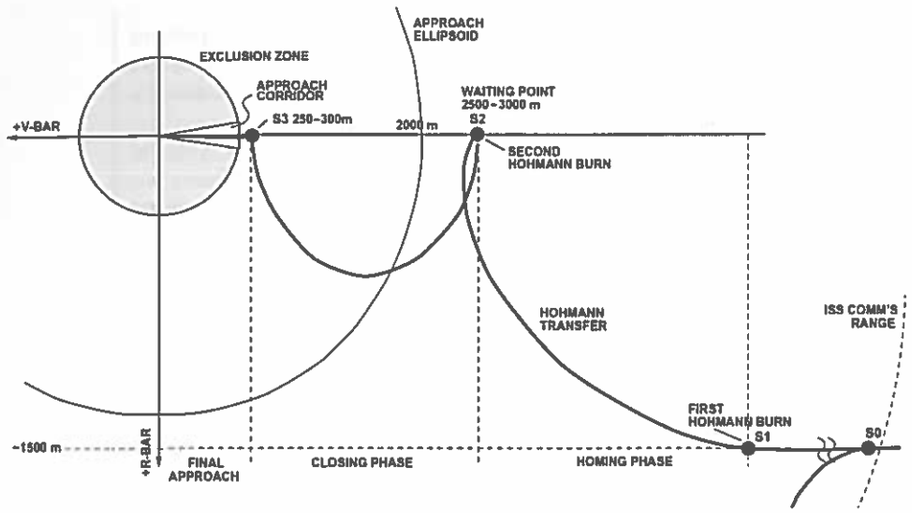

Figure 8.33 ISS stable orbit approach on −V-bar as typically adopted by an ATV rendezvous. First, a Hohmann transfer brings the interceptor to the waiting point S2. Then, it approaches the ISS on an elliptical trajectory to waiting point S3.

So, for +V-bar approach of a "safety-first" rendezvous with the ISS as shown in Figure 8.29 and Figure 8.33, the ellipse maneuver is used. As shown in Section 8.5.3, in particular Figures 8.24 and 8.25, a vertical (radial) burn v_0 will bring us on an ellipse to the next waiting point S3 that lies by $\Delta x = \text{S2}-\text{S3} = 4v_0/n < 0$, with $\text{S2} < 0, \text{S3} < 0$, closer to the target. When arriving at S3, a reverse burn must be fired to bring the interceptor to a halt. For the required delta-v for such a step of width Δx, we find from Figure 8.25

$$\Delta v = \pm 2 \times \frac{\Delta x}{4}\sqrt{\frac{\mu}{a^3}} \quad @ \text{ elliptic trajectory} \tag{8.6.6}$$

where the factor 2 indicates that we need two burns for the entire approach maneuver and the ± sign that the elliptic trajectory might be on either side of the V-bar. This maneuver can be performed at any step size and as often as wanted to get to S3. Observe that it does not make any difference for the total delta-v if a given distance is covered with more or less steps because $\Delta v \propto \Delta x$. How many increments are to be chosen is just a matter of safety and time (every step lasts one orbital period). So, if Δx is the total distance between S2 and S3, Eq. (8.6.6) provides the delta-v for the entire closing transfer independent of the number of steps. To approach the ISS, every incremental distance of 1 km requires $\Delta v = 2 \times 0.286\ \text{m s}^{-1}$.

If the cycloidal approach would be chosen, we have from Figure 8.22 $\Delta x = 6\pi v_0/n$ and hence

$$\Delta v = \pm 2 \times \frac{\Delta x}{6\pi \cdot k}\sqrt{\frac{\mu}{a^3}} \quad @ \text{ cycloidal trajectory} \tag{8.6.7}$$

where Δx is the total distance between S2 and S3 and k is the number of cycloidal revolutions to traverse this distance. Here again the factor 2 indicates that we need a initiation burn at S2 plus a stop burn of equal absolute value at S3. We therefore see that the cycloidal approach is by a factor $6\pi \cdot k/4 = 4.7 \cdot k$ more efficient that the elliptic approach—at the expense of safety. We recall that every cycloidal or elliptic cycle takes a full orbital period.

Approach to +V-bar

If one wants to approach on the −V-bar from S2 to the waiting point S3 on the +V-bar, i.e., to the other side of the target, one has to apply the same maneuvers (elliptic or cycloidal trajectories) as above, the only difference being that for $\Delta x = \text{S2}-\text{S3} < 0$ holds $\text{S2} < 0, \text{S3} > 0$.

Approach to ±R-bar

If the final approach is on +R-bar or −R-bar, the closing phase must bring the interceptor in a loop from −V-Bar to ±R-bar (see Figure 8.34) at below/above the target. Here again both the cycloidal and the elliptic trajectory would do, but here both approaches are equally safe. This is because if control is lost for a cycloidal trajectory, it would just pass by the target at the aimed distance and after that drift away from the target. In the elliptic trajectory case, the interceptor would just orbit the target on an

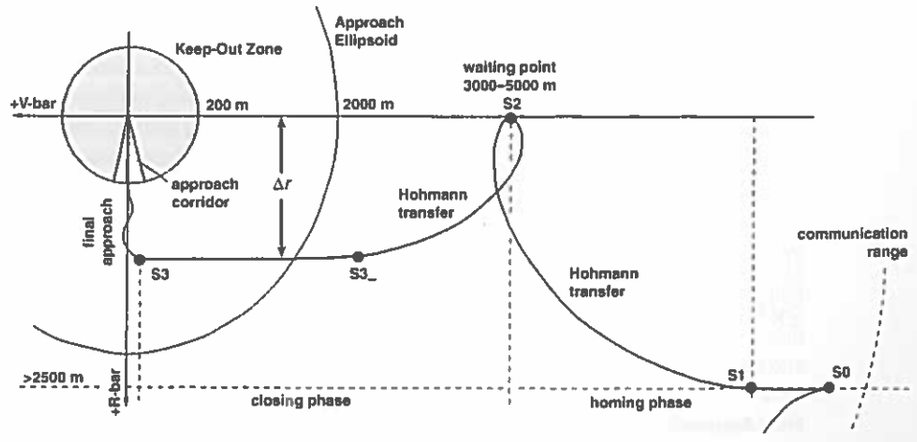

Figure 8.34 To +R-bar approach to ISS. A Hohmann transfer brings the interceptor first to the intermediate point S3_, where it crosses over into a circular orbit on which it drifts to the final point S3.

ellipse. Because we have seen that the cycloidal trajectory is much more efficient, it is the preferred approach method.

The cycloidal loop is performed in two (or one) steps. First, a tangential burn Δv brings the interceptor on a prolate cycloid (Hohmann trajectory) to the transition point S3_ where a burn Δv is fired against the direction of movement. This brings the interceptor into a circular Earth orbit below/above the ISS. On this orbit, it slowly drifts to the point S3 below the ISS from where the final approach commences. Note that neither S3_ nor S3 are stable points with respect to the ISS. If the first burn is accurate enough, it can be set such that S3_ coincides with S3.

What needs to be determined is: Given the initial point S2 and a radial distance Δr (counted positively outward along the z-axis) the interceptor shall dive below ($\Delta r < 0$) or above ($\Delta r > 0$) the ISS, what is the delta-v to perform the entire maneuver? From Figure 8.22 we derive that the diving distance is $\Delta r \equiv \Delta z = 4v_0/n$. We therefore find for the initial delta-v

$$\Delta v_i = \frac{\Delta r}{4}\sqrt{\frac{\mu}{a^3}} \quad \text{@ initial burn} \tag{8.6.8}$$

Upon diving down/up, the interceptor speeds up and according to Eq. (8.5.11) achieves at the lowest/highest point of the trajectory, which is S3_, the relative velocity $\dot{x} = v_0(4\cos\pi - 3) = -7v_0$. This corresponds in an Earth centered system to

$$v_- = \sqrt{\frac{\mu}{a}} - 7v_0$$

At $r = a + \Delta r$, the anticipated circular orbit has an orbital velocity of

$$v_+ = \sqrt{\frac{\mu}{a+\Delta r}} = \sqrt{\frac{\mu}{a}}\left(1 - \frac{1}{2}\frac{\Delta r}{a}\right) = \sqrt{\frac{\mu}{a}} - 2v_0$$

where the latter follows by applying Eq. (8.6.8). For the delta-v of the braking burn at S3_, we therefore obtain

$$\Delta v_f = v_- - v_+ = -5v_0 \tag{8.6.9}$$

So the total delta-v is

$$\Delta v = |\Delta v_i| + |\Delta v_f| = 6 \times \frac{\Delta r}{4}\sqrt{\frac{\mu}{a^3}}$$

Thus, while for the -V-bar approach our effort to get to S3 is maximally $\Delta v = 2|v_0|$ (elliptic trajectory), it is much bigger, namely, $\Delta v = 6|v_0|$, in the case of an approach to ±R-bar.

8.6.5 Final Approach

The interceptor is now on the waiting point S3 just outside of the Keep-Out Sphere, about 200 m away from the ISS (see Figure 8.35). This is where the *final approach* (a.k.a. *proximity operations or terminal phase*) begins. Other than during the stable orbit rendezvous where the interceptor approached the target via stable orbits (i.e., cycloidal trajectories that can be stopped at the reversal points or elliptic trajectories that even back off from the target if rendezvous control is lost and therefore are "safe" orbits), the trajectories now are more or less straight to directly intercept the target and therefore are on "collision course" with it. The final approach ends at a distance of a few meters upfront the ISS, either when docking is imminent or when the target is within capture distance of the manipulator. During this phase, the spacecraft usually maneuvers autonomously, i.e., without intervention by ground control. The spacecraft control loop must therefore be closed locally, either by the crew or by the automatic controllers. Final approach can thus be considered the most critical part of the R&D mission. During this phase, minor errors can cause accidents.

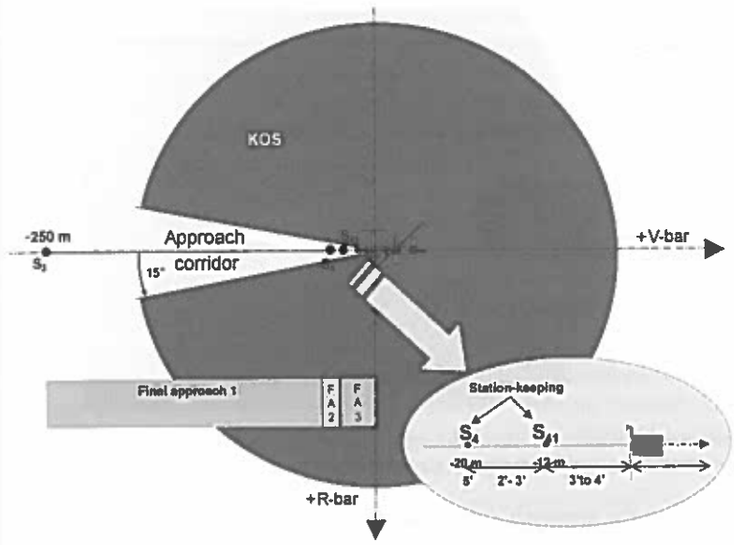

Figure 8.35 ISS approach corridor for V-bar approach.

±V-bar Approach

First, we consider the approach on +V-bar or on −V-bar (see definition of "±V-bar approach" in the section "*LVLH* Reference System" above) from waiting point S3 through the conical approach corridor with half angle 15° to the next waiting point S4 (the initial waiting point for docking approach). To penetrate the cone, one could continue to apply the ellipse maneuvers. However, every incremental step takes one orbital period of 91.5 min in case of the ISS, which is far too much.

One therefore switches to another approach mode called *forced translation*. Figure 8.36 shows its principle. Let us assume a burn is performed aiming directly at the target. According to Figure 8.22, the higher speed would force the interceptor to drift upward (centrifugal force is bigger than the gravitational force at this circular

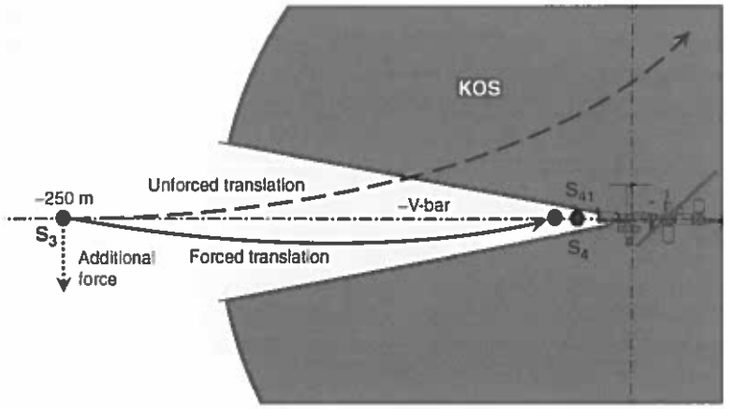

Figure 8.36 A straight trajectory would turn up and leave the approach corridor. A downwards forced translation enforces the trajectory to stay in the corridor and hit the waiting point.

altitude), violate the approach cone, and never encounter S4 (see Figure 8.36). However, we can counteract the updrift by providing in addition to the forward translation an initial small downward force. If this is done properly, it forces the initial trajectory slope down just that the trajectory at its end hits S4. The forward translation with this extra little downward force is called *forced translation*.

It needs to be determined how big the additional delta-v, equivalent to the downward force, is. We therefore revisit Section 8.5.3, where we have shown that for translation times $(nt)^2 \ll 1$ (Eqs. (8.5.10)) holds. These equations give the answer to the question what the initial velocity $v_0 = (\dot{x}_0, \dot{y}_0, \dot{z}_0)$ at the initial point (x_0, y_0, z_0) should be in order to meet after time t a given target point at the origin $(0, 0, 0)$. In our case, the vector from the target point to the initial distance of the interceptor is $(x_0, y_0, z_0) = (\pm\Delta x, 0, 0)$ for a $\pm$V-bar approach. Therefore, Eq. (8.5.10) reduces to

$$v_0 = (v_{0x}, v_{0y}, v_{0z}) = \left(\mp\frac{\Delta x}{t}, 0, \pm n \cdot \Delta x\right) \quad @\ \pm\text{V-bar approach} \tag{8.6.10}$$
$$\Delta v = v_0 - v_i$$

where $n = \sqrt{\mu/a^3}$, Δv is the initiation burn vector, and v_i is the interceptor's velocity incident to the starting point S3 (if the starting point was a waiting point, $v_i = 0$). Of course, for braking the forced translation at S4, the same amount of Δv is required, however, for v_{0x} into the opposite direction. The initial speed in x direction, v_{0x}, is easy to grasp: The required speed is distance divided by flight time. The delta-v in negative z direction (radial thrust downward) is just the forced part. Assuming that the delta-v in each direction is generated by separate thrusters (as usually the case), the absolute value of the total approach delta-v is

$$\Delta v = 2\left(\frac{\Delta x}{t} + n \cdot \Delta x\right) = 2 \cdot \Delta x \cdot \left(\frac{1}{t} + n\right)$$

It would not be wise to cover the final approach distance in one move. Initial point and firing errors would jeopardize encountering exactly the target point. One rather splits

the distance into two or more parts and whenever the trajectory meets the V-bar, a new forced delta-v of $\pm 2 \times n \cdot \Delta x$ is applied starting the forced translation anew. This leads to a hopping approach as depicted in Figure 8.37 (top) for a Shuttle + V-bar approach. This is why it is called *hooping trajectory*. Because the total delta-v has the linear dependency $\Delta v \propto \Delta x$, it does not make any difference in terms of delta-v effort to split the final approach distance into k shorter hops of length ε, $\Delta x = k \cdot \varepsilon$, but still cover the total distance in the same time t, or not. However, owing to boost errors, it is preferable to make more shorter hops.

±R-bar Approach

Forced translation can also be applied on the +R-bar or −R-bar, which, for instance, is performed by a Soyuz or Progress docking to the radial port (Pirs docking compartment) of the ISS. This approach was originally designed for docking the Shuttle with MIR. It was also used on Hubble servicing mission STS-82. To determine the initiating delta-v for the forced translation from S3 to S4, we have from Eq. (8.5.10) with the initial distance vector $(0, 0, \mp\Delta z)$ for ±R-bar approach

$$v_0 = (v_{0x}, v_{0y}, v_{0z}) = \left(\pm n \cdot \Delta z, 0, \pm\frac{\Delta z}{t}\right) \quad @\ \pm\text{R-bar approach} \tag{8.6.11}$$
$$\Delta v = v_0 - v_i$$

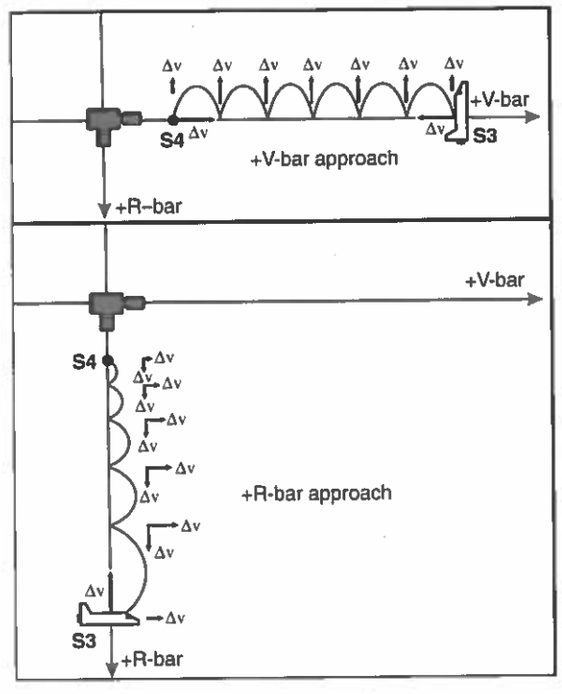

Figure 8.37 Final approach hopping profiles of a Shuttle final approach along the + V-bar (above) and the + R-bar (below, including deceleration burns).

where $n = \sqrt{\mu/a^3}$, Δv is the initiation burn vector, and v_i is the interceptor's velocity incident to the starting point S3. The total approach delta-v is by the same token as above

$$\Delta v = 2 \cdot \Delta z \left(\frac{1}{t} + n \right)$$

And also in this case owing to the linear dependency $\Delta v \propto \Delta z$, it does not make any difference in terms of delta-v effort to split the distance into more shorter hops. Thus, we might have also hopping trajectories as shown in Figure 8.37 (bottom).

Proximity Operations

From an orbital mechanics point of view, the last few meters starting out from S4, the docking approach in the proximity of the target, is the most easy part of the rendezvous. This is because for very short distances $x, z, \tau \rightarrow 0$ and hence

$$\begin{aligned} v_{0x} &= -\frac{x_0}{t} - nz_0 \\ v_{0z} &= -\frac{z_0}{t} + nx_0 \\ v_{0y} &= -\frac{y_0}{t} \end{aligned} \longrightarrow \begin{aligned} v_{0x} &= -\frac{x_0}{t} \\ v_{0z} &= -\frac{z_0}{t} \\ v_{0y} &= -\frac{y_0}{t} \end{aligned} \qquad (8.6.12)$$

$$\Delta v = (v_{0x}, v_{0y}, v_{0z}) - v_i$$

where v_i is the interceptor's velocity incident to the starting point S4. Therefore, if on this docking approach the commander or pilot navigates the interceptor, steering becomes intuitively easy because the required momentary speed is just distance per time. However, in order not to crash into the docking port, the approach speed has to be continuously reduced (see Figure 8.37, bottom).

Docking/Capture Phase

At the end of the final approach phase, the interceptor is in position in front of the target's docking port or capture interface and all thrusting has ceased. The interceptor's relative velocity is either zero for capture and berthing, or slightly above zero for docking. On the one hand, this approach rate must be great enough to prevent the vehicles from bouncing off each other without capture being achieved. On the other hand, it must be low enough to prevent structural damage or loss of control and/or the ability to attenuate the momentum. The exact position, velocity, orientation, and angular rate tolerances depend on the specific docking or capture tools being used.

The docking/capture phase is the conclusion of a R&D mission. It encompasses the following activities:

- docking/capture of the target by the interceptor (or vice versa)
- establishment of a rigid structural connection
- connection of fluid, gas, electrical, propellant, and communication lines
- establishment of a pressurized passageway if crew transfer is part of the mission goals.

Docking means that the active spacecraft positions itself and establishes the physical connection using its own momentum. In capture and berthing, the target or interceptor is captured, positioned, and connected by a robotic manipulator to a berthing mechanism. Berthing thus allows contact to be made at a near-zero cloture rate, which means a higher level of control for the operator, and avoids the process of one vehicle basically flying into the other. It is therefore the generally preferable approach, but comes at the cost of requiring a complex, heavy, and expensive *Remote Manipulator System* (RMS).

8.6.6 Shuttle-ISS Rendezvous

The Shuttle's close range rendezvous with the ISS is somewhat different, though, because the docking port is on the leading side (+V-bar) of the ISS. Therefore, beginning at S2 the Shuttle flies in two cycloidal steps and within two orbits a homing approach from S2 to S3 such that it dives just below the ISS (see Figure 8.38). Note that the launch window was chosen such that daytime (i.e., sunlight) condition is at those parts of the trajectory, including the final approach and docking

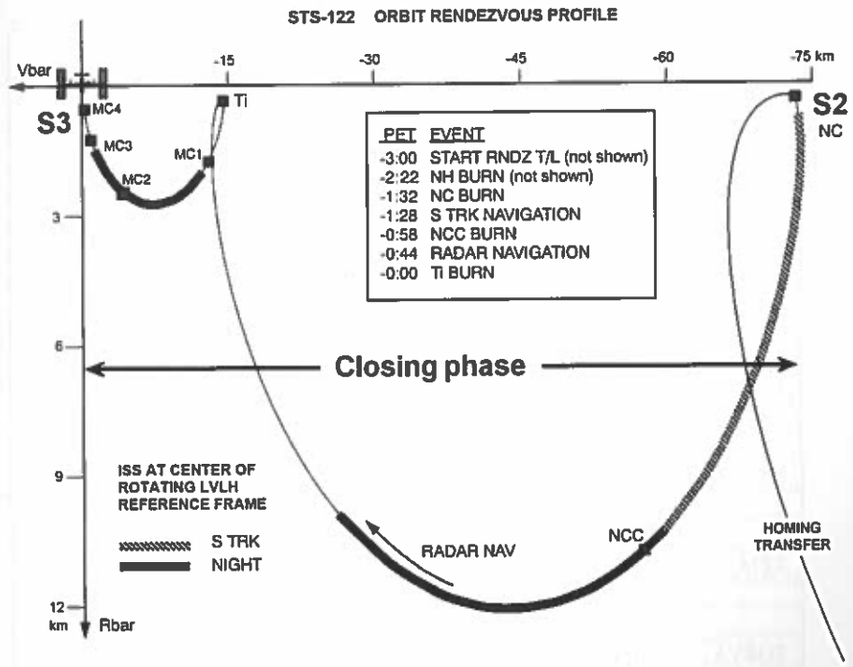

Figure 8.38 The cycloidal trajectory in the closing phase of a Shuttle STS-122 rendezvous with the ISS.

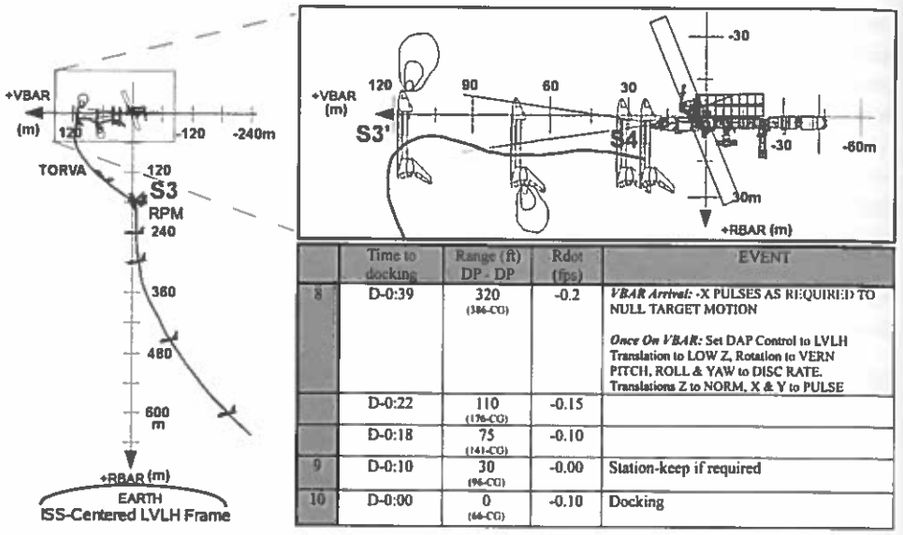

	Time to docking	Range (ft) DP - DP	Rdot (fps)	EVENT
8	D-0:39	320 (386-CG)	-0.2	*VBAR Arrival:* -X PULSES AS REQUIRED TO NULL TARGET MOTION *Once On VBAR:* Set DAP Control to LVLH Translation to LOW Z, Rotation to VERN PITCH, ROLL & YAW to DISC RATE. Translations Z to NORM, X & Y to PULSE
	D-0:22	110 (176-CG)	-0.15	
	D-0:18	75 (141-CG)	-0.10	
9	D-0:10	30 (96-CG)	-0.00	Station-keep if required
10	D-0:00	0 (66-CG)	-0.10	Docking

Figure 8.39 Final approach trajectory of the Shuttle STS-122 approaching the ISS.

Acronyms for NASA Rendezvous Maneuvers

NC	(Phasing correction burn) Performed to hit a range relative to the target at future times
NH	(Height adjust burn) Performed to hit a delta-height relative to target at future times
NPC	(Plane change burn) Performed to remove planar errors relative to target at future times
NCC	(Corrective combination burn) First on-board targeted burn in the rendezvous sequence to reduce phasing and height errors relative to the target at Ti
Ti	(Terminal intercept burn) Second on-board targeted burn in the rendezvous sequence to place the orbiter on a trajectory to intercept the target in one orbit
MC-1, 2, 3, 4	(Midcourse correction burns) On-board targeted burns to correct the post Ti trajectory in preparation for the final approach phase
RPM	(Rendezvous Pitch Maneuver) A 360° backflip that allows the station crew to take pictures from the Zvezda Service Module of the Shuttle's heat shield
TORVA	(Twice Orbital Rate R-bar to V-bar Approach) This manually performed maneuver brings the orbiter from the + R-bar to the + V-bar

(see Figure 8.39), where the ISS needs to be seen from the Shuttle and vice versa. Just before arriving at S3, the commander of the Shuttle takes over manual control for the remainder of the approach and docking. He will stop the Shuttle at S3 some 180 m below the ISS and will maneuver the Shuttle through a 9 min, 360° backflip (a.k.a. *Rendezvous Pitch Maneuver*, RPM) that allows the station crew to take pictures of the Shuttle's heat shield to see whether it was damaged during launch. The commander then will move the Shuttle in the so-called TORVA maneuver from the + R-bar to the + V-bar in a position about 120 m directly in front of the station in preparation for the final approach to the pressurized mating adapter PMA-2 located at the leading end of the US utility hub *Harmony*.

8.6.7 Plume Impingement

The term *plume impingement* covers all effects exerted on the target object if it is impacted by the exhaust gases of the interceptor's reaction control system (the maneuvering control system of an interceptor) thrusters. One of these effects is the plume pressure force acting on the target and causing position and attitude disturbances. Another is the heat load placed on the target's structure by the hot gases. This can lead to overheating of parts of the surface and the underlying structure. The third effect is the contamination of the target's surfaces by combustion products and unburned propellant components. This can cause contamination of not only sensitive elements on the target's surfaces, particularly optical elements such as camera lenses, solar arrays, or docking sensors, but also sealing elements of the docking mechanism. This risk of contamination must be considered in particular during orbit servicing missions such as Hubble servicing, where these considerations impacted the design of final approach trajectories.

Therefore, plume impingement is one of mission planners' major concerns during proximity operations, apart from collision avoidance and maneuver precision. It can only be avoided if thruster activity near the target is minimized. This in turn means that the interceptor's relative velocity must diminish below a threshold value as it approaches the target. During Gemini and Apollo, plume impingement never became a significant issue due to the thrust magnitude, the position and canting of the RCS nozzles, as well as the roughly equal sizes of interceptor and target and the absence of large appendages such as solar arrays. This changed during the Skylab missions. During Skylab 2, the Apollo *Command and Service Module* (CSM) was maneuvered within close proximity so that a crewman standing in the hatch could reach the stuck solar array with a deployment tool. The CSM thrusting to null the closing velocity triggered Skylab AOCS to fire its jets in order to maintain its attitude. This resulted in an opening rate between the two vehicles. On the later Apollo–Soyuz Test Mission, four of the CSM's thrusters were inhibited 2 s prior to docking contact in order to prevent plume loading of the Soyuz solar arrays.

Space Shuttle

These lessons were carried into the Space Shuttle design process. The massive orbiter is designed to assemble and maintain large space stations and service comparatively small and light satellites. These are equipped with large solar arrays and antennas or sensitive optics. Plume impingement therefore is a prime concern. The size of the Shuttle was predetermined by the payload it was designed to carry and the location of RCS thrusters by its shape, which in turn was determined by the requirements of re-entry and atmospheric flight. Plume impingement concerns could therefore be addressed only by careful design of R&D approaches.

The underlying assumptions were as follows: The target spacecraft could not be designed with features preventing contamination (e.g., movable sensor covers as found on Hubble), and the control of the target attitude could not prevent contamination. Therefore, on each mission a target-dependent minimum range existed, at which the thrusters could still be fired in the direction of the target without contamination concern. At the minimum range, the orbiter was to transition from a direct approach trajectory to a station-keeping point on the V-bar (see Figure 8.40). From this point on the final approach would be flown in forced translation. A number of such approaches were planned for the Shuttle's *Long Duration Exposure Facility* (LDEF) mission. Simulations showed that an Apollo-type inertial approach and braking technique would cause LDEF to tumble. In addition, plume impingement induced dynamics at grapple ranges that could make both LDEF deployment and retrieval difficult.

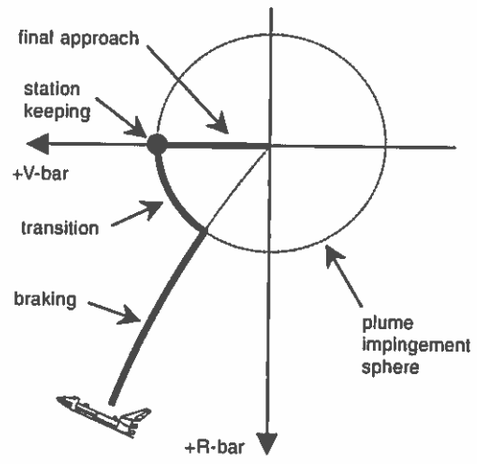

Figure 8.40 Approach profile to avoid plume impingement on target. When the approaching interceptor reaches the border of a plume impingement sphere, it performs a transition maneuver to a station-keeping point on the V-bar following the borders of the plume impingement sphere. After the station-keeping point is reached, the interceptor flies a forced translation final approach.

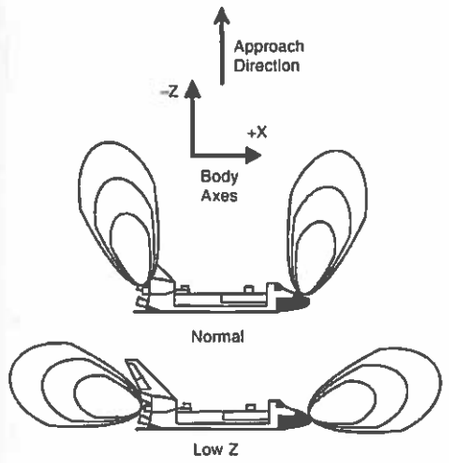

Figure 8.41 Space Shuttle Low-Z RCS mode. The orbiter's thrusters are fired only in the Shuttle's longitudinal axis (*x*-axis). This significantly reduces plume impingement. On the other hand, owing to the canting of the thrusters, this provides minimal braking capability in the forward *z* direction.

Another countermeasure for plume impingement issues specific to the Space Shuttle was the development of the *Low-Z* approach. In this approach, all forward firing RCS jets are inhibited, with all thrust thus acting primarily along the spacecraft's longitudinal *x*-axis (see Figure 8.41). All braking thrust in the *z* direction therefore results from the canting of the longitudinal thrusters. This provides minimal RCS braking capability, while minimizing RCS plume impingement. It is also expensive in terms of propellant use. Notwithstanding its limitations, *Low-Z* mode has been employed on satellite servicing missions, including Hubble servicing, and the missions to MIR and ISS.

Problems

Problem 8.1 Adjacent Circular Orbit Approximation

Prove Eq. (8.3.8)

$$\frac{\sqrt{a_\bullet}+\sqrt{a_\circ}}{\sqrt{a_H}}-1 \approx 1-\frac{1}{16}\left(\frac{a_\circ-a_\bullet}{a_\bullet}\right)^2 \quad @\ a_\circ \to a_\bullet$$

Problem 8.2 Transfer between Aligned Ellipses

Consider a Hohmann transfer between two coplanar and coaxial ellipses. Show that the propulsion demand for the transition between the periapsis of the inner ellipse and the apoapsis of the outer ellipse is